Progress In Electromagnetics Research, Vol. 134, 289–299, 2013

A WIDEBAND AND DUAL-RESONANT TERAHERTZ METAMATERIAL USING A MODIFIED SRR STRUCTURE

Wanyi Guo[1, 2, *], Lianxing He[1], Biao Li[3], Teng Teng[1, 2], and Xiaowei Sun[1]

[1]Key Laboratory of Terahertz Solid-State Technology, Shanghai Institute of Microsystem and Information Technology, Shanghai 200050, China

[2]Graduate University of the Chinese Academy of Sciences, Beijing 100049, China

[3]National Laboratory of Antennas and Microwave Technology, Xidian University, Xi'an, Shaanxi 710071, China

Abstract—We present the desgin, fabrication and measurment of a dual-resonant broadband terahertz (THz) matamterial based on a modified split-ring resonator (MSRR) structure. The proposed MSRR is constructed by connecting the inner split ring with the outer split ring of adjacent cell. Transmission and reflection characteristics of the proposed structure are simulated using Ansoft HFSS, and the permittivities show negative values in 0.492–0.693 THz and 0.727–0.811 THz bands. The designed sample is fabricated on a gallium arsenide layer, and experiments are performed in Terahertz Time-Domain Spectroscopy. Measured transmission characteristics agree well with the simulations.

1. INTRODUCTION

Metamaterials are engineered materials with negative effective permittivity and/or permeability, which owe their properties mainly to sub-wavelength details of structure rather than to their chemical compositions [1]. Due to the fascinating performances, the new class of materials can dramatically add a degree of freedom to control of electromagnetic waves. As a result, the emergence of metamaterials

Received 23 October 2012, Accepted 22 November 2012, Scheduled 26 November 2012

* Corresponding author: Wanyi Guo (gwynh@mail.sim.ac.cn).

has attracted significant attention in THz regime, where natural materials perform weak electric and magnetic response [2, 3]. The first experimental realization of THz metamaterial was reported by T. J. Yen et al. in 2004 [4]. From then on, a variety of THz metamaterial-based functional devices have been realized, including intelligent switches, sensors, modulators, absorbers and so on [5–7]. For example, an efficient active metamaterial switch/modulator operating at THz frequencies was presented by Hou-Tong Chen et al. in 2006 [5]. And a high sensitivity terahertz chemical and biochemical sensors was reported by Christian Debus et al. in 2007 [6]. Hu et al. presented a metamaterial that acts as a strongly resonant absorber with an experimental absorptivity of 70% at 1.3 THz [7]. However, due to the resonant nature of SRR-type metamaterials, the potential functions are restricted in single and narrow frequency range, which limit the practical applications for broadband and multi-band operations. In order to solve this problem, a few methods to broaden the bandwidth and realize multi-resonance operation have been proposed [8–14]. A hybrid SRR metamaterial design is proposed to provide a novel approach to realize tunable and broadband THz response for the THz detection sensitivity enhancement [9]. A multi-layer metamaterials provides a promising way to extend SRR based metamaterial operating region from narrow band to broadband [10]. And a tunable multi-band metamaterial design can be realized using micro-split SRR structures [13].

In this letter, we present a new and simple way to broaden the bandwidth of the SRR based metamaterial. The modified split-ring resonator (MSRR) is constructed by connecting the inner split ring with the outer split ring of the next cell. The proposed metamaterial reveals two distinct strong resonances at ~ 0.515 THz and ~ 0.74 THz, respectively. Compared to the convetional split-ring resonator (CSRR), the MSRR provides one more resonance by adding a connection line between the neighbouring SRR unit cells. Additionally, the absolute frequency bandwidths with negative permittivity are greatly enhanced.

2. DESIGN AND ANALYSES

Figures 1(a) and (b) show the structures of CSRR and the proposed MSRR, respectively. MSRR is constructed by connecting the inner split ring with the outer split ring of the next cell. The periodicity of the metallic sub-wavelength structures is carefully chosen to be 58 μm and 64 μm in two perpendicular directions respectively to achieve electro/magnetic (EM) resonance in THz regime. The whole structure

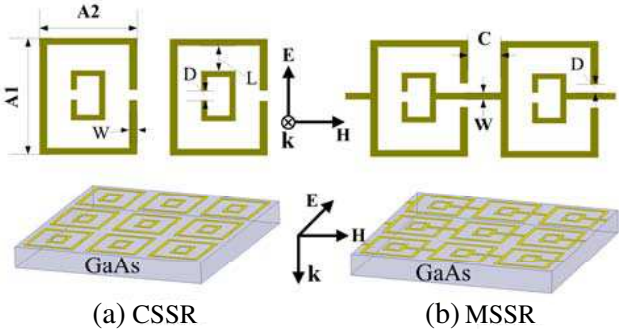

Figure 1. The designed structures of CSRR and MSRR.

is constructed on a 20-μm-thick gallium arsenide (GaAs) substrate with a dielectric constant ε of 12.9 and a loss tangent $\tan\delta$ of 0.006, and the metal array layer is gold with the thickness of 300 nm. The THz wave propagates at normal incidence (k in Fig. 1) with the mutually orthogonal electric and magnetic fields lying completely on the parallel plane to the metal arrays. And the polarization of the THz electric field is perpendicular to the capacitive gap (E in Fig. 1). The CSRR/MSRR structures are simulated and optimized by the finite element-based commercial electric and magnetic fields solver Ansoft HFSS. And the designed geometrical sizes are as follows: $W = 3\,\mu\text{m}$, $L = 12\,\mu\text{m}$, $A1 = 52\,\mu\text{m}$, $A2 = 46\,\mu\text{m}$, $C = 12\,\mu\text{m}$, $D = 4\,\mu\text{m}$.

The simulated magnitude and phase results of transmission (S_{21}) and reflection (S_{11}) parameters of both CSRR and MSRR are presented in Figs. 2(a) and (b). As one can see that, there is only one transmission valley with phase mutation near 0.7 THz in CSRR, while two transmission valleys with phase mutation near 0.515 THz and 0.74 THz are presented in MSRR. In addition, the minimum of S_{21} magnitude at the additional transmission valley of MSRR is -33 dB, which is 9 dB lower than the minimum value of S_{21} magnitude of CSRR at 0.7 THz. So one may presume that resonance enhancement is achieved due to the additional connecting metal bar in MSRR.

Based on a two ports network and using the methods mentioned in [15], the effective relative permittivity and permeability can be obtained from the complex refractive index n and wave impedance z (where $k = \omega/c$, ω is radian frequency, d is the slab thickness, and c

is the speed of light.):

$$\varepsilon = \frac{n}{z} = \varepsilon' + i\varepsilon'', \quad \mu = nz = \mu' + i\mu'' \tag{1}$$

$$n = \frac{1}{kd}\cos^{-1}\left[\frac{1}{2S_{21}}\left(1 - S_{11}^2 + S_{21}^2\right)\right] \tag{2}$$

$$z = \sqrt{\frac{(1+S_{11})^2 - S_{21}^2}{(1-S_{11})^2 - S_{21}^2}} \tag{3}$$

Using the formulas above, the effective medium parameters are extracted and shown in Figs. 2(c)–(f). For CSRR, the real part of effective permittivity performs negative values in the frequency band of 0.701–0.799 THz, the absolute and relative (to the centre frequency) bandwidths are 98 GHz and 13.07% respectively, which is corresponding to the transmission valley with phase mutation. While for MSRR, the real part of effective permittivity performs negative values in two frequency bands of 0.492–0.693 THz and 0.727–0.811 THz. At the first resonance point near 0.515 THz of MSRR, the absolute and relative bandwidths are 201 GHz and 33.9% respectively, which is nearly double of the bandwidth in CSRR. The added connection bar between the neighbouring SRR unit cells help to provide an additional resonance with wider frequency band. At the second resonance point near 0.74 THz of MSRR, the absolute and relative bandwidths are 84 GHz and 10.92% respectively, which is similar to the resonance at 0.7 THz of CSRR. And the real and imaginary parts of permeability of CSRR and MSRR are shown in Fig. 2(f).

It is observed that the MSRR is effective in broadening the bandwidth and realizing dual-band resonance of THz metamaterial. Additionally, the minimum of relative permittivity at the first resonance of MSRR is about -170, which is much lower than the minimum relative permittivity (about -38) of CSRR. The much stronger resonance of MSRR with high negative permittivity is expected to improve the sensitivity and reliability for metamaterial-based devices such as intelligent switches, sensors, modulators and absorbers.

The different electrical responses of CSRR and MSRR to the electromagnetic wave of normal incidence can be analyzed by the surface current distribution, which is shown in Fig. 3 under the same current color bar. The black arrows denote the directions of surface current, and different colors demonstrate the different current densities. Fig. 3(b) shows the induced surface current at the electrical resonance frequency point of 0.7 THz of CSRR. The much smaller current density at 0.515 THz of CSRR shown in Fig. 3(a) implies that the electrical

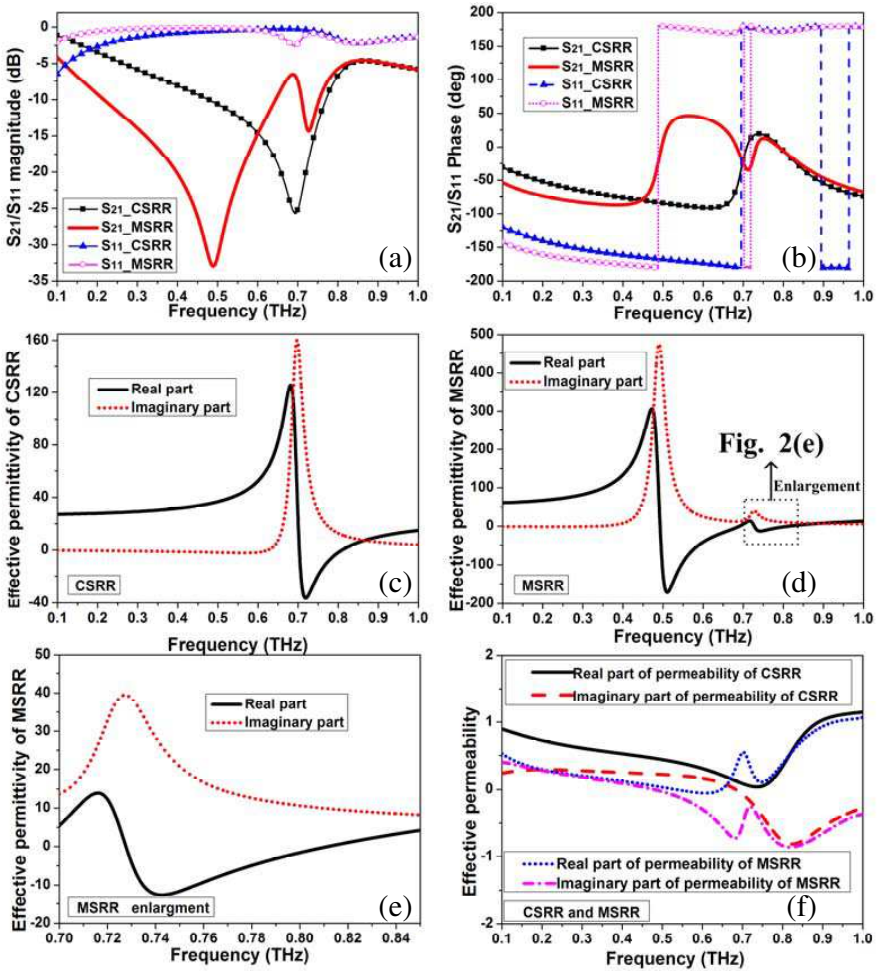

Figure 2. Simulation results of CSRR and MSRR. (a) Magnitude of transmission (S_{21}) and reflection (S_{11}); (b) Phase of S_{21} and S_{11}; (c) Effective permittivity of CSRR; (d) Effective permittivity of MSRR. (e) The enlargement of the dashed box in Fig. 2(d). (f) The effective permeability of CSRR and MSRR.

resonance has not been effectively excited and the permittivity cannot reach the negative values regime. From the Figs. 3(b) and (d), one can see that the surface current of CSRR at 0.7 THz is almost the same as that of MSRR at 0.74 THz. So the bandwidth and strength of the two resonances are similar, which is verified by Fig. 2. Compared with Figs. 3(c) and (b)/(d), one can see that the induced surface current

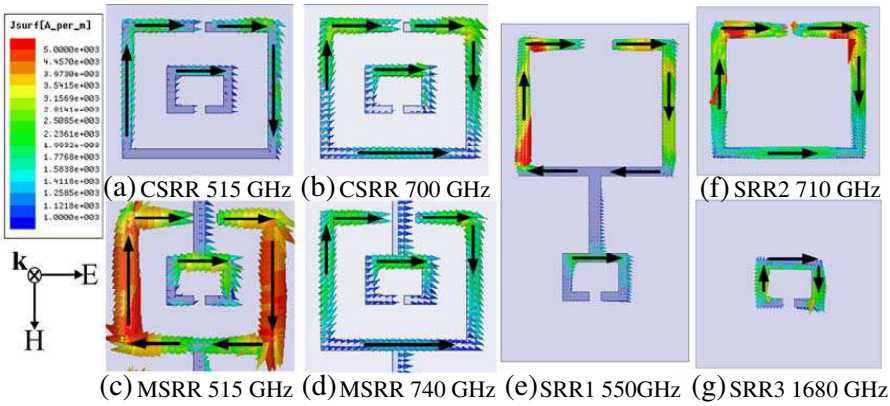

Figure 3. Surface current distribution of CSRR and MSRR. (a) CSRR at 515 GHz; (b) CSRR at 700 GHz; (c) MSRR at 515 GHz; (d) MSRR at 740 GHz; (e) SRR1 at 550 GHz; (f) SRR2 at 710 GHz; (g) SRR3 at 1680 GHz.

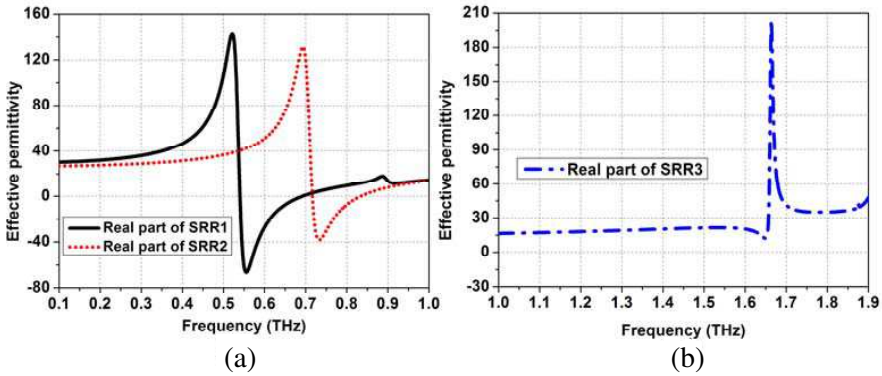

Figure 4. Simulated transmission lines: (a) SRR1 and SRR2; (b) SRR3.

distribution on the outer split ring of MSRR at 0.515 THz is circular, and its density is much larger than the others, leading to a stronger electrical resonance and wider frequency band with higher negative permittivity.

The presence of the metallic bar connecting between two adjacent SRR unit cells modifies the transmission spectra significantly. To better understand the function of the added connecting metallic bar, the resonance properties of the unit cell components denoted as SRR1,

SRR2 and SRR3 are analyzed. As shown in Figs. 3(e)–(g), SRR2 is the outer split ring of CSRR, SRR3 is the inner split ring of the CSRR, and SRR1 is the connection of SRR2 and SRR3 using a metallic bar. Figs. 4(a) and (b) show that the three structures resonate at ~ 550 GHz (SRR1), ~ 710 GHz (SRR2), and ~ 1680 GHz (SRR3), respectively. Being constructed by placing SRR3 in SRR2, CSRR resonates at ~ 700 GHz, which is mainly contributed to the resonance of SRR2. While SRR1 is constructed by connecting SRR2 and SRR3 using a metallic bar. The resonance of SRR1 (~ 550 GHz) are contributed to both SRR2 and SRR3, and the added connecting line has enhanced the effect of SRR3. Considering the similarity of surface current distribution and resonance frequency, one may presume that the resonance of MSRR at 515 GHz is mainly originated from SRR1. And the resonance of MSRR at 740 GHz is probably originated from SRR2, which shows the similarity of the resonance of CSRR at 700 GHz.

3. FABRICATION AND MEASUREMENT

In order to verify the design and simulation results, the metal planar array pattern of CSRR and MSRR were fabricated using photolithography and magnetron sputtering. To form the planar array pattern, S6809 of Shipley Co. and FHD320 of Fujifilm Co. were used as photoresist and developing solution, respectively. Samples were first soaked in chlorobenzene for 5 minutes before developing, which made them easier for liftoff. Then three metal layers Au/Pt/Ti with the thickness of 300/20/20 nm were deposited on the 350-µm-thick gallium arsenide (GaAs) substrate by magnetron sputtering. The titanium layer was used to ensure a good adhesion to substrate, the platinum layer placed between titanium and gold was used to prevent the possible intermetallic diffusion. Liftoff technology was used to remove the unnecessary metals. Each sample was realized in $5\,\mathrm{mm}^2$. The SEM images of a portion of the fabricated samples are shown in Figs. 5(a) and (b).

The performance of the fabricated metamaterial samples was characterized by the Terahertz Time-Domain Spectroscopy (THz-TDS) in a dry nitrogen atmosphere at room temperature. All experiments were performed at normal incidence, with the mutually orthogonal electric and magnetic fields lying completely on the parallel plane to the metal arrays. And the polarization of the THz electric field was perpendicular to the capacitive gap (E in Fig. 1). Frequency-domain results were obtained by Fourier transform from the time-domain signal in the THz-TDS experiments. As illustrated in Figs. 6(a)

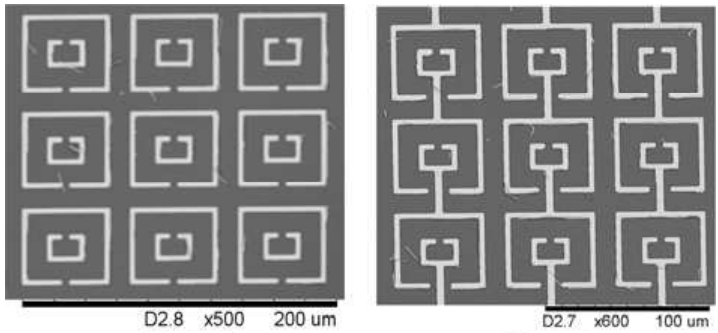

Figure 5. The SEM images of a portion of the fabricated metamaterial samples based on CSRR and MSRR.

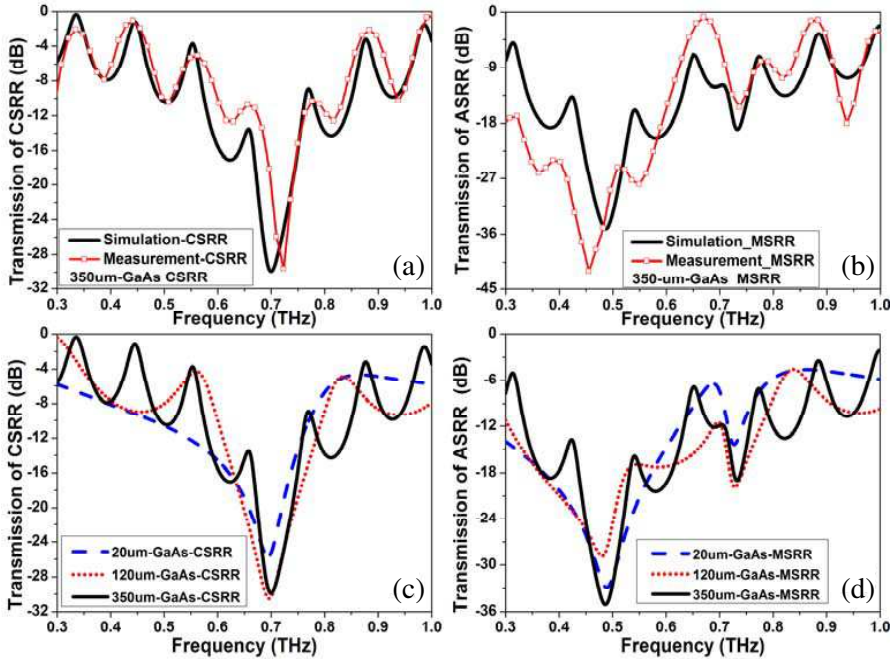

Figure 6. The measurements of CSRR and MSRR. (a) Measured and simulated transmission of CSRR. (b) Measured and simulated transmission of MSRR. (c) Simulated transmission of different thickness substrates for CSRR. (d) Simulated transmission of different thickness substrates for MSRR.

and (b), measured and simulated results are in good agreement.

As mentioned in [12, 16, 17], the substrates with different thicknesses affect the transmission spectra. The simulated transmission lines of CSRR and MSRR with 20-/120-/350-μm-thick GaAs substrates are plotted in Figs. 6(c) and (d). A few ripples in the transmission spectra come from the Fabry-Perot resonances [10, 18], which are caused by the internal reflections within the two surfaces in the direction of propagation. To better study the resonant nature of the metal sub-wavelength structure, the Fabry-Perot resonance frequency should be far away from the designed frequencies with metamaterial performance. So we analyse the metamaterial with metal layers constructed on the 20-μm-thick GaAs substrate, where the Fabry-Perot resonance frequency is separated from the as-designed metamaterial frequency. While considering the fabrication conditions and difficulties in measurement, we fabricated the metal layers with designed sub-wavelength structures on the 350-μm-thick GaAs substrate, and do the measurement successfully. Good agreement is achieved between the simulated and measured results.

4. CONCLUSIONS

In summary, we present a dual-resonant broadband THz metamaterial using a MSRR structure. The proposed MSRR exhibits two strong electric resonances at 0.515 THz and 0.74 THz. Negative values of permittivity in frequency bands of 0.492–0.693 THz and 0.727–0.811 THz are achieved. The bandwidth with negative permittivity of MSRR near 0.515 THz is almost double that of CSRR near 0.7 THz. Additionally, much stronger resonance with a high negative permittivity of -170 (much lower than -38 of CSRR) is also excited by MSRR, which is expected to improve the sensitivity and reliability of functional devices based on metamaterials. The proposed MSRR structure, as a simple modification to CSRR, is meaningful in broadening the bandwidth, realizing dual-band operations, and improving the resonance strength.

ACKNOWLEDGMENT

This work was supported by the National Basic Research Program of China (973) (Grant No. 2009CB320207).

REFERENCES

1. Veselago, V. G., "The electrodynamics of substances with simultaneously negative values of ε and μ," *Sov. Phys. Usp.*, Vol. 10, No. 4, 509–514, 1968.
2. Chen, H.-T., W. J. Padilla, M. J. Cich, A. K. Azad, R. D. Averitt, and A. J. Taylor, "A metamaterial solid-state terahertz phase modulator," *Nature Photonics*, Vol. 3, 148–151, 2009.
3. Han, J., A. Lakhtakia, and C.-W. Qiu, "Terahertz metamaterial with semiconductor split-ring resonators for magnetostatic tenability," *Opt. Express*, Vol. 16, No. 19, 14390–14396, 2008.
4. Yen, T. J., W. J. Padilla, N. Fang, D. C. Vier, D. R. Smith, J. B. Pendry, D. N. Basov, and X. Zhang, "Terahertz magnetic response from artificial materials," *Science*, Vol. 303, No. 5663, 1494–1496, 2004.
5. Chen, H.-T., W. J. Padilla, J. M. O. Zide, A. C. Gossard, A. J. Taylor, and R. D. Averitt, "Active terahertz metamaterial devices," *Nature*, Vol. 444, No. 7119, 597–600, Nov. 2006.
6. Christian, D. and H. B. Peter, "Frequecncy selective surfaces for high sensitivity terahertz sensing," *App. Phys. Lett.*, Vol. 91, No. 18, 184102(1)–184102(3), Aug. 2007.
7. Tao, H., N. I. Landy, C. M. Bingham, X. Zhang, R. D. Averitt, and W. J. Padilla, "A metamaterial absorber for the terahertz regime: Design, fabrication and characterization," *Opt. Express* Vol. 16, No. 10, 7181–7188, 2008.
8. Wen, Q.-Y., H.-W. Zhang, Y.-S. Xie, Q.-H. Yang, and Y.-L. Liu, "Dual band terahertz metamaterial absorber: Design, fabrication, and characterization," *App. Phys. Lett.*, Vol. 95, No. 24, 16527–16534, 2009.
9. Lim, C. S., M. H. Hong, Z. C. Chen, N. R. Han, B. Luk'yanchuk, and T. C. Chong, "Hybrid metamaterial design and fabrication for terahertz resonance response enhancement," *Opt. Express*, Vol. 18, No. 12, 12421–12429, 2010.
10. Han, N. R., Z. C. Chen, C. S. Lim, B. Ng, and M. H. Hong, "Broadband multi-layer terahertz metamaterials fabrication and characterization on flexible substrates," *Opt. Express*, Vol. 19, No. 8, 6991–6998, 2011.
11. Yuan, Y., C. Bingham, T. Tyler, S. Palit, T. H. Hand, W. J. Padilla, D. R. Smith, N. M. Jokerst, and S. A. Cummer, "Dual-band planar electric metamaterial in the terahertz regime," *Opt. Express*, Vol. 16, No. 13, 9746–9752, 2008.
12. Yuan, Y., C. Bingham, T. Talmage, S. Palit, T. H. Hand,

W. J. Padilla, N. M. Jokerst, and S. A. Cummer, "A dual-resonant terahertz metamaterial based on single-particle electric-field-coupled resonators," *App. Phys. Lett.* Vol. 93, No. 19, 19110(1)–19110(3), 2008.

13. Ekmekci, E., K. Topalli, T. Akin, and G. Turhan-Sayan, "A tunable mult-band metamaterial design using micro-split SRR structures," *Opt. Express*, Vol. 17, No. 18, 16406–16058, 2009.
14. Han, J. G., J. Q. Gu, X. C. Lu, M. X. He, Q. R. Xing, and W. L. Zhang, "Broadband resonant terahertz transmission in a composite metal-dielectric structure," *Opt. Express*, Vol. 17, No. 19, 036617(1)–(11), 2005.
15. Smith, D. R., D. C. Vier, T. Koschny, and C. M. Soukoulis, "Electromagnetic parameter retrieval from inhomogeneous metamaterials," *Phys. Rev. E*, Vol. 71, 036617(1)–(11), 2005.
16. Chen, Z. C., N. R. Han, Z. Y. Pan, Y. D. Gong, T. C. Chong, and M. H. Hong, "Tunable resonance enhancement of multi-layer terahertz metamaterials fabricated by parallel laser micro-lens array lithography on flexible substrates," *Opt. Materials Express*, Vol. 1, No. 2, 151–157, 2011.
17. Ng, B., S. M. Hanham, V. Giannini, Z. C. Chen, M. Tang, Y. E. Liew, N. Klein, M. H. Hong, and S. A. Maier, "Lattice resonances in antenna arrays for liquid sensing in the terahertz regime," *Opt. Express*, Vol. 19, No. 15, 14653–14661, 2011.
18. Liu, X.-X., D. A. Powell, and A. Alu, "Correcting the Fabry-Perot artifacts in metamaterial retrieval procedures," *Phys. Rev. B*, Vol. 84, No. 23, 235106(1)–(7), 2011.